JACS
JOURNAL OF THE AMERICAN CHEMICAL SOCIETY
pubs.acs.org/JACS
Article

Zn Microenvironment Engineering for Aryl-C(sp^2) Cleavage to Phenols and Tertiary Amines

Lulin Wang,[#] Yike Huang,[#] Yu Xin, Tianjiao Wang, Sen Luan, Minghua Dong, Bin Zhang, Xiaojun Shen, Qinglei Meng, Buxing Han, and Huizhen Liu*

Cite This: J. Am. Chem. Soc. 2025, 147, 37255−37264
Read Online
ACCESS | Metrics & More | Article Recommendations | Supporting Information

ABSTRACT: Cleaving inert aryl-C(sp^2) bonds present a fundamental catalytic challenge due to their intrinsic robustness, yet it is essential for valorizing lignin into value-added chemicals. Current strategies predominantly convert aromatic rings to phenols at the expense of side-chain carbon utilization, compromising the atom economy. We report zinc coordination microenvironment engineering to achieve efficient aryl-C(sp^2) cleavage in phenolic substrates with transformable side chains (e.g., ketones and alkenes), concurrently yielding phenols and tertiary amines. A nitrogen-coordinated zinc catalyst (ZnNC-900) delivered 90.0% phenol and 82.7% N,N-dimethylethylamine from 4-methoxyacetophenone. Significantly, this catalytic system demonstrates broad activity toward multiple native lignin sources, with bamboo lignin processing on a 5.0 g scale affording 1.04 g of alkyl-free phenolics (20.8 wt %) and 0.67 g of N,N-dimethylethylamine (13.4 wt %). Mechanistic studies via spectroscopy and DFT calculations demonstrate that the zinc microenvironment dictates the reaction pathway. Specifically, the ZnNC-900 catalyst, featuring zinc coordinated by three pyrrolic-N atoms and one pyridinic-N atom, reduces the energy barrier by 0.71 eV relative to ZnNC-600 (which exclusively has pyridinic-N coordination). This work provides a catalytic strategy to overcome the limitations of low atom economy, harsh conditions, and narrow substrate scope in lignin valorization.

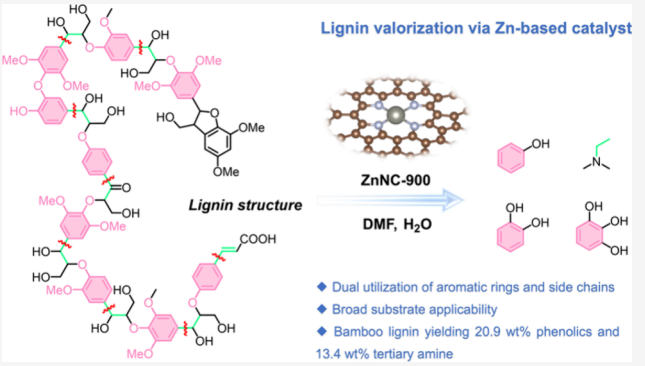

INTRODUCTION

The selective cleavage of robust carbon−carbon (C−C) bonds is pivotal to advancing synthetic chemistry, enabling access to high-value compounds for applications ranging from pharmaceuticals to sustainable materials.[1−7] While homogeneous catalysts have achieved notable success in activating strained C−C bonds (e.g., alkyl, alkenyl, and alkynyl) via redox-active metals or nonmetals,[8−11] the inert nature of unstrained aryl-C(sp^2) σ-bonds remains a critical unsolved challenge due to their thermodynamic stability and lack of intrinsic activation pathways. This limitation is acutely exemplified in lignin valorization, where the selective scission of aryl-C(sp^2) bonds could unlock lignin—Earth's largest renewable aromatic reservoir—as a sustainable alternative to alkyl-free phenolic compounds like phenol.[12−17] The global market for phenol is projected to reach 14.5 million tons by 2030.[18] Currently, phenol production relies overwhelmingly on coal tar and petroleum-based processes, underscoring the urgency of developing catalytic strategies to convert lignin's inert bonds into renewable aromatic building blocks.

Existing strategies for lignin depolymerization involving the cleavage of aryl-C(sp^2) σ-bonds always suffer from two intrinsic trade-offs: (i) harsh conditions that compromise energy efficiency, and (ii) neglect of side-chain valorization, resulting in carbon loss as CO_2 or low-value alkanes.[19−23] For instance, zeolites demonstrate exceptional performance in dealkylating lignin oil to yield both phenol and propylene,[20] showcasing the potential to convert both aromatic nuclei and side chains into valuable products.[21] However, these dealkylation reactions typically require elevated temperatures, reaching up to 410 °C.[21] Alternative approaches, such as the oxidation-hydrogenation route developed by Wang et al., achieve aryl-C(sp^2) σ-bonds cleavage but often result in the conversion of alkyl chains into low-value CO_2.[22] Acid-catalyzed processes using HCl, H_2SO_4, and HY have also been reported,[15,21,23] yet they fall short of harnessing lignin's full potential as a versatile platform for aromatic nuclei and side chains—a necessary condition for atom-efficient biorefineries.

Received: June 20, 2025
Revised: September 23, 2025
Accepted: September 23, 2025
Published: October 2, 2025

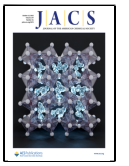

https://doi.org/10.1021/jacs.5c10429
J. Am. Chem. Soc. 2025, 147, 37255−37264

Scheme 1. Cleavage of Aryl-C(sp^2) Bonds to Phenols and Tertiary Amines

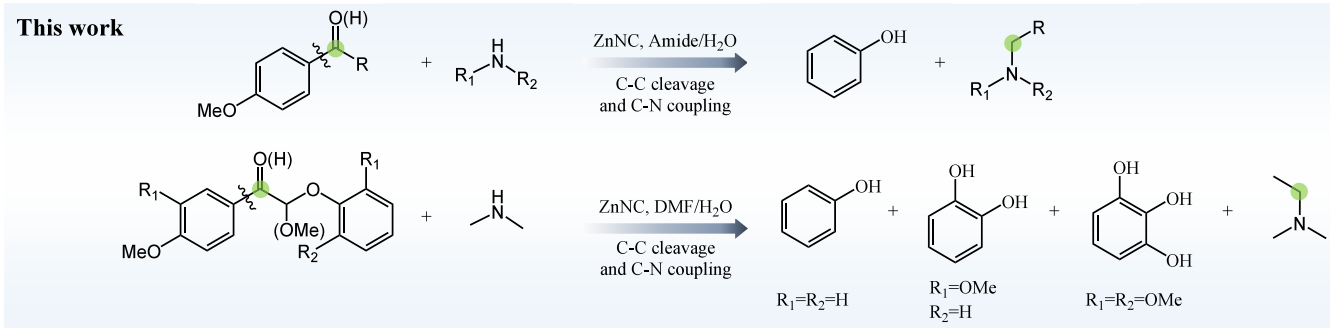

Table 1. Optimization of the Reaction Conditions[a]

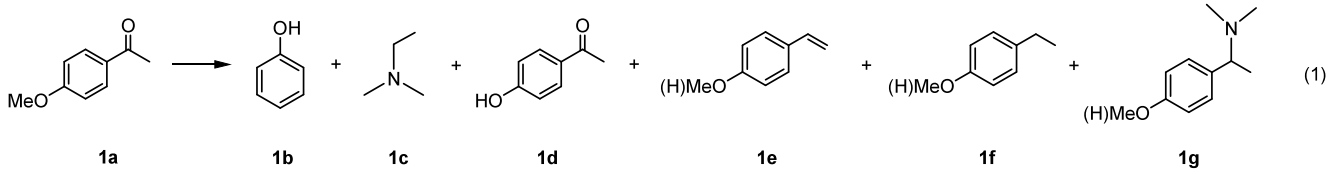

Entry	Catalyst	Conv. (mol %)	Yield (mol %)					
			1b	1c	1d	1e	1f	1g
1	Blank	82.0	41.6	29.7	8.5	4.5	0.8	3.7
2	ZnNC-900	100.0	90.0	82.7	2.5	0.0	0.5	0.0
3	NC-900	79.0	41.9	36.9	20.7	6.2	0.6	6.9
4	$ZnCl_2$	82.6	35.2	34.3	20.5	0.7	0.8	0.0
5[b]	ZnNC-900 (No DMA)	66.2	35.3	35.5	13.2	11.0	0.0	4.7
6[c]	ZnNC-900 (No H_2O)	<0.8	0.0	0.0	0.0	0.0	0.0	0.0
7[d]	ZnNC-900 (H_2)	No reaction						

[a]Reaction conditions: 4-methoxyacetophenone (0.4 mmol), catalyst (10 mg), N_2 (1 MPa), 200 °C, 6 h. The qualitative analysis of the product was determined by mass spectrometry, and the conversion of substrate and the yield of products were determined by GC with dodecane as internal standard. DMF (2 mL), 40 wt % DMA in H_2O (2 mL). [b]DMF (2 mL), H_2O (2 mL). [c]20 wt % DMA in THF (4 mL). [d]H_2O (4 mL), H_2 (1 MPa).

To address these challenges, it is essential to devise a strategy that allows for the cleavage of aryl-C(sp^2) σ-bonds while simultaneously functionalizing the side chains. This method would facilitate the simultaneous transformation of both aromatic rings and side chains into high-value chemicals. Given the importance of amine and phenolic compounds, developing a technique for converting lignin into phenols (derived from the aromatic rings) and alkyl amines (derived from the side chains) is crucial. Here, we propose a strategy that employs small-molecule aliphatic amines as mediators to enhance the cleavage of aryl-C(sp^2) σ-bonds in various substrates, thereby facilitating the production of phenols and alkyl amines under the catalysis of nitrogen-coordinated zinc catalyst (Scheme 1). Under optimized conditions, ZnNC-900 achieved 92.6% phenol and 71.3% N,N-dimethylethylamine (DME) yields from the lignin model compound 1-(4-methoxyphenyl)-2-phenoxyethanone. When applied to the transformation of native lignin, the yields of phenol and dimethylethylamine (DME) can reach 20.8 and 13.4 wt %, respectively. By combination of X-ray absorption fine structure (XAFS), X-ray photoelectron spectroscopy (XPS), and DFT calculations, we reveal that Zn sites coordinated by three pyrrolic-N atoms and one pyridinic-N atom in ZnNC-900 stabilize key intermediates (e.g., C═N^+ Schiff base) through electron engineering, significantly reducing the C−C cleavage barrier to 1.38 eV compared to ZnNC-600 catalysts. This work establishes a new paradigm for efficient and total valorization of lignin to value-added chemicals.

RESULTS AND DISCUSSION

Catalytic Performance. The cleavage of aryl-C(sp^2) bonds was initially investigated using 4-methoxyacetophenone as a model substrate. As shown in Table 1, the catalytic performance was evaluated in a solvent system composing N, N-dimethylformamide (DMF), dimethylamine (DMA), and deionized water (denoted as DMF-DMA-H_2O) at 200 °C for 6 h under a nitrogen atmosphere. In the absence of any catalyst (entry 1, Table 1), the substrate achieved 82% conversion, yielding phenol (41.6%, Product **1b**) and N,N-dimethylethylamine (DME, 29.7%, Product **1c**) as primary products, alongside minor byproducts including 1-(4-hydroxyphenyl)-ethanone (8.5%, Product **1d**), styrene derivatives (4.5%, Product **1e**), ethylbenzene-type compounds (0.8%, Product **1f**), and addition products (3.7%, Product **1g**). Introducing ZnNC-900[24] as the catalyst (entry 2) dramatically enhanced performance, achieving 100% substrate conversion with phenol and DME yields of 90.0% and 82.7%, respectively, while suppressing byproducts (0.5% Product **1f**). Control experiments revealed the critical role of ZnNC-900's unique composition: replacing it with NC-900 (entry 3) or $ZnCl_2$ (entry 4) resulted in significantly lower phenol and DME yields (<50%) and increased undesired byproducts (>20% Product **1d** and 5−10% Product **1e** or **1g**), highlighting the synergistic interplay between zinc species and the carbon matrix in ZnNC-900. The solvent system was further optimized through a systematic component exclusion.

https://doi.org/10.1021/jacs.5c10429
J. Am. Chem. Soc. 2025, 147, 37255−37264

Table 2. Influence of the Calcination Temperature on ZnNC-X[a]

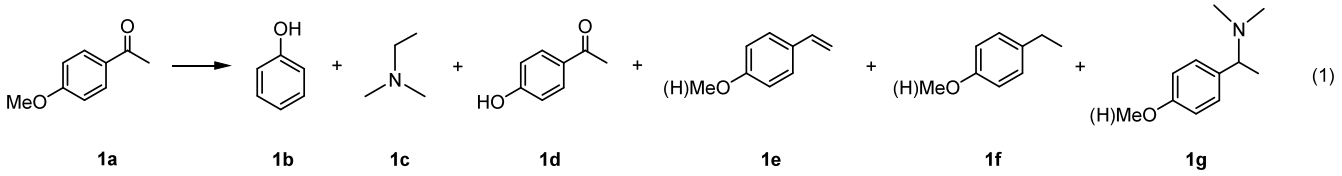

Entry	Catalyst	Conv.(mol %)	Yield (mol %)					
			1b	1c	1d	1e	1f	1g
1	ZnNC-500	98.5	42.0	46.7	35.5	5.0	3.8	4.0
2	ZnNC-600	100	45.1	49.4	35.2	5.8	2.4	4.3
3	ZnNC-700	100	55.7	59.1	24.4	6.1	3.4	3.6
4	ZnNC-800	100	54.0	58.4	20.4	6.4	7.3	0.0
5	ZnNC-900	100	90.0	82.7	2.5	0.0	0.5	0.0
6	ZnNC-1000	100	42.6	46.2	26.8	6.4	10.7	0.0

[a]Reaction conditions: 4-methoxyacetophenone (0.4 mmol), ZnNC-X (10 mg), DMF (2 mL), 40 wt % DMA in water (2 mL), N_2 (1 MPa), 200 °C, 6 h.

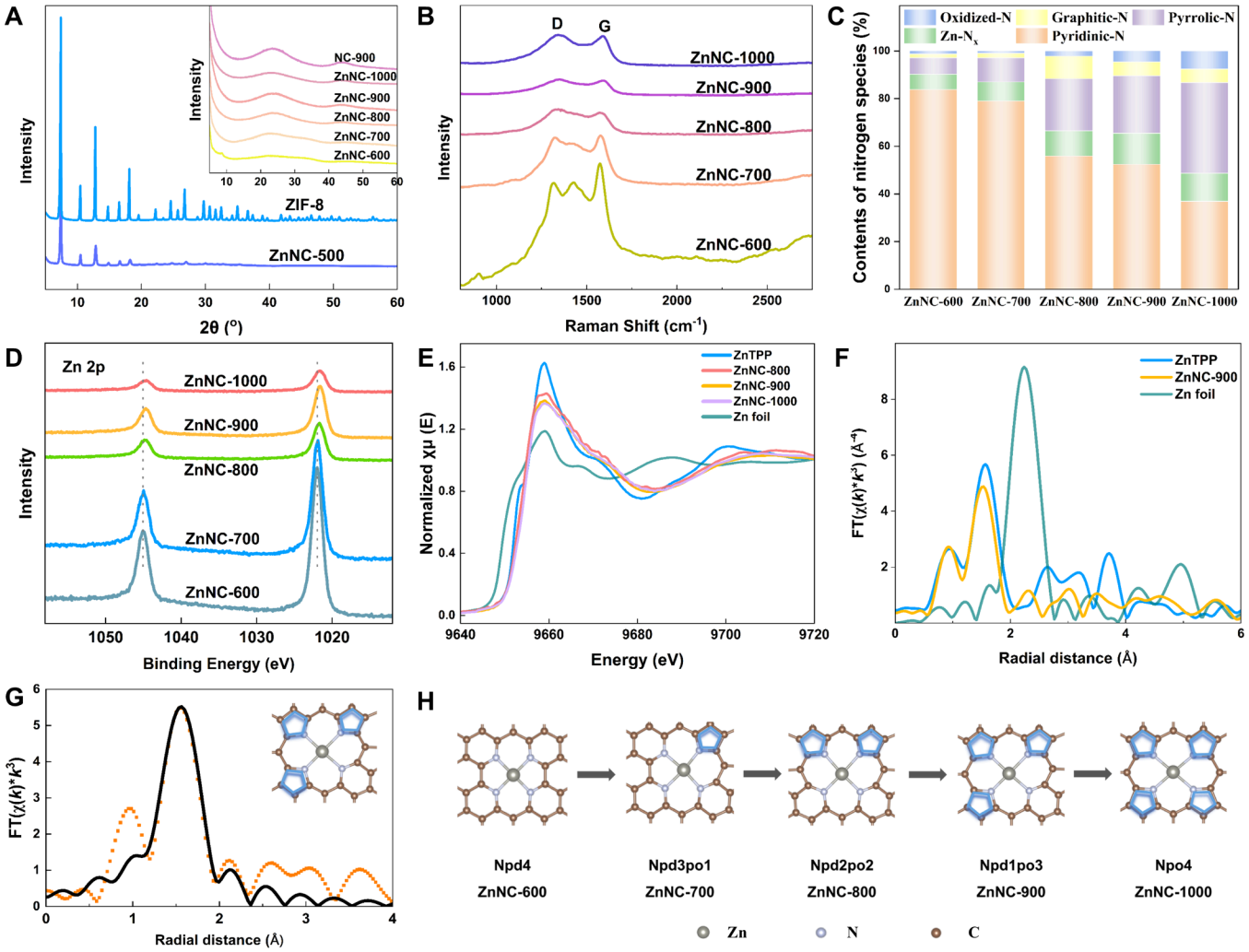

Figure 1. Structural characterization of ZnNC-X catalysts. (A) The XRD pattern. (B) The Raman spectra. (C) The contents of the various nitrogen species in ZnNC-X samples. (D) Zn 2p XPS spectra for ZnNC-X catalysts. (E) Zn K-edge XANES spectra of ZnTPP, ZnNC-800, ZnNC-900, ZnNC-1000 and Zn foil. (F) Fourier transformed (FT) k^3 weighted Zn K-edge EXAFS spectra of ZnTPP, ZnNC-900 and Zn foil. (G) Zn K-edge EXAFS (points) and the fitting curve (line) of ZnNC-900, are shown in R-space. The data are k^3-weighted and not phase-corrected. (H) Structural changes from ZnNC-600 to ZnNC-1000.

Removing DMA (Entry 5) reduced substrate conversion to 66.2%, with phenol and DME yields dropping to 35.3% and 35.5%, respectively, while incomplete cleavage byproducts (Products **1d**−**1g**) surged. Omitting H_2O (entry 6) nearly

https://doi.org/10.1021/jacs.5c10429
J. Am. Chem. Soc. 2025, 147, 37255−37264

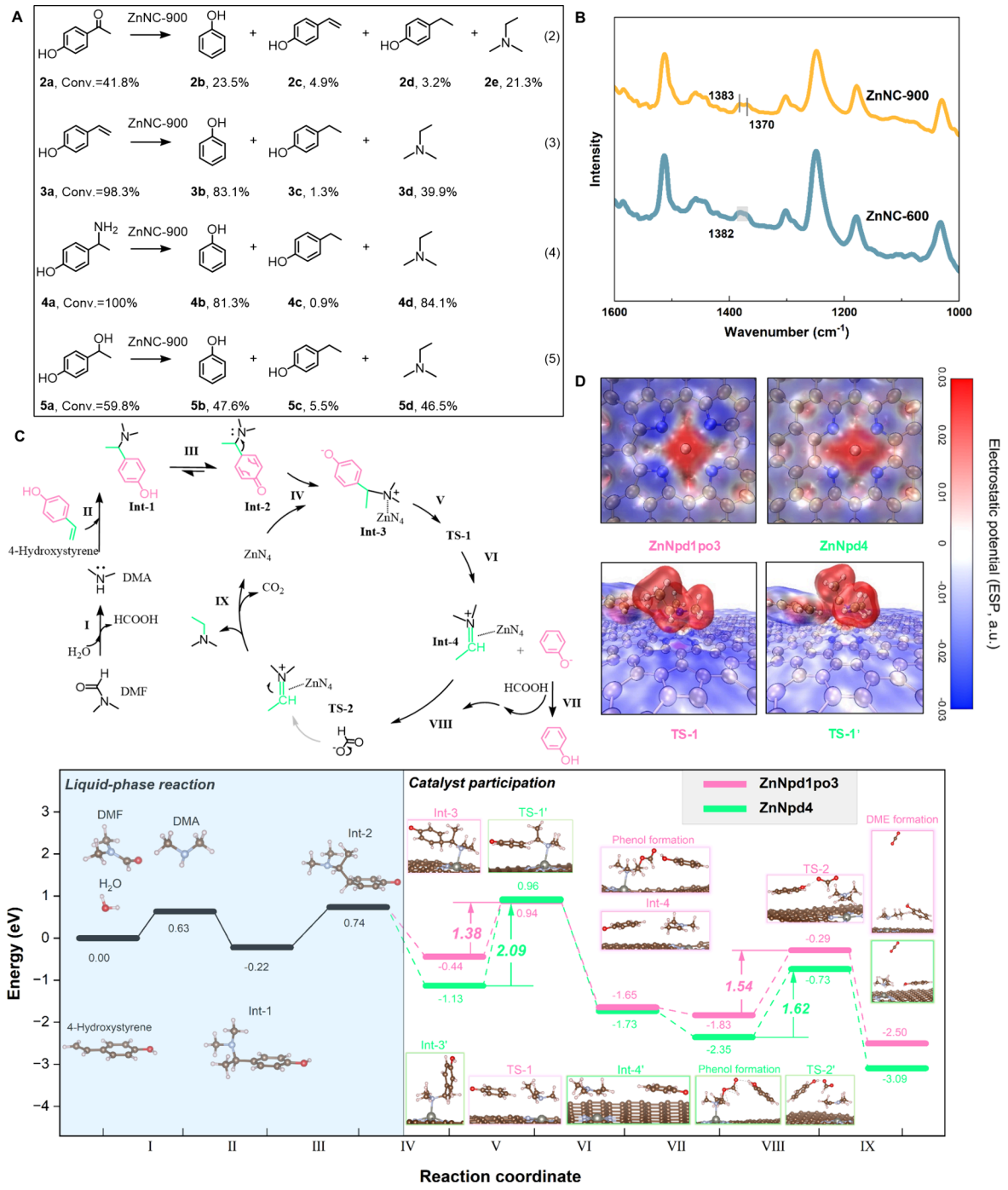

Figure 2. Mechanism exploration. (A) Selective hydrogenation of different possible intermediates. Reaction conditions: substrate (0.4 mmol), ZnNC-900 (10 mg), DMF (2 mL), 40 wt % DMA (2 mL), N_2 (1 MPa), 200 °C, 2h. (B) FTIR spectra of 4-(1-aminoethyl)phenol adsorption on ZnNC-600 and ZnNC-900. (C) Reaction mechanism and potential energy diagram for aryl-C(sp^2) cleavage in 4-vinylphenol over ZnNpd1po3 and ZnNpd4. Calculations were carried out at the level of PBE-D3(BJ)/ DZVP-MOLOPT-GTH-SR. (D) ESP mapped on electronic density isosurface with isovalue 0.0075 e $a.u.^{-3}$ (C: brown, N: blue, Zn: sliver, H: white, O: red. Negative ESP value is indicated by blue, and positive by red).

abolished reactivity (<1% conversion), underscoring its essential role in hydrogen transfer. Replacing DMF/DMA with molecular hydrogen (entry 7) resulted in no substrate conversion, confirming the solvent system's irreplaceable function in hydrogen donation. Besides, we evaluated the stability of ZnNC-900 through cycling tests. The results show that the yields of phenol and DME remained above 75% after used four times (Figure S3). These results collectively demonstrate that the DMF-DMA-H_2O system, coupled with ZnNC-900, provides an optimal microenvironment for efficient aryl-C(sp^2) bond activation and selective C−N coupling.

To systematically probe the impact of catalyst structure on performance, we synthesized a series of ZnNC-X materials (X = calcination temperature, 500−1000 °C) via pyrolysis of ZIF-8 and evaluated their activity under optimized conditions (Table 2, entries 1−6). While all catalysts calcined above 500 °C achieved complete substrate conversion, ZnNC-900

https://doi.org/10.1021/jacs.5c10429
J. Am. Chem. Soc. 2025, 147, 37255−37264

uniquely stood out, delivering phenol and DME yields of 90.0% and 82.7% with minimal side-chain retention (0.5% Product **1f**). In contrast, catalysts pyrolysis at other temperatures (500−800 or 1000 °C) exhibited significantly lower efficiencies (40−50% phenol/DME yields) and substantial accumulation of byproducts with side chains (e.g., **1d**, about 30%).

Catalyst Characterization. To unravel the structural and electronic evolution of ZnNC-X catalysts with the pyrolysis temperature, we integrated XRD, elemental analysis, Raman spectroscopy, XPS, and XAS. XRD patterns (Figure 1A) reveal that ZIF-8 retains its crystalline structure at 500 °C, evidenced by persistent sharp peaks. At higher temperatures (600−1000 °C), these peaks diminish, replaced by broad reflections at 26° and 44°-assigned to the (002) and (101) planes of graphitic carbon-signaling progressive carbonization.[25] Elemental analysis (Table S1) further tracks compositional shifts: carbon content rises steadily from 41.2% (500 °C) to 84.4% (1000 °C), while nitrogen and zinc decline. Notably, ZnNC-500 retains 21.3% Zn, mirroring pristine ZIF-8, confirming limited decomposition at 500 °C. Zinc volatilization intensifies near its boiling point (907 °C), reducing Zn content to <5% in ZnNC-1000. In contrast, Zn-free NC-900 exhibits distinct composition (42.3% C, 21.5% N). Raman spectra (Figure 1B) detail the carbon defect dynamics. ZnNC-600 shows three peaks: a D band (1330 cm^{-1}, disordered carbon), amorphous carbon (1500 cm^{-1}), and a G band (1590 cm^{-1}, graphitic carbon). Above 700 °C, the amorphous carbon signal weakens, while D and G band intensities rise. The increasing I_D/I_G ratio (0.98 to 1.12) with temperature confirms enhanced defect density, aligning with XRD's graphitization trends.

XPS analysis of N 1s spectra (Figures S4) resolves five nitrogen types:[26] pyridinic-N (398.5 eV), Zn−N_x (399.8 eV), pyrrolic-N (400.6 eV), graphitic-N (401.3 eV), and oxidized-N (402.0 eV). With increasing pyrolysis temperature (600 to 1000 °C), pyridinic-N content dropped sharply from 83.8% to 36.9%, while pyrrolic-N and oxidized-N rose from 6.9% to 38.0% and 1.4% to 7.6%, respectively (Figure 1C, Table S2, Figure S4). Zn−N_x and graphitic-N displayed a volcano trend, peaking at ZnNC-900. Parallel Zn 2p XPS analysis (Figure 1D) revealed binding energy downshifts for Zn $2p_{1/2}$ (1045 to 1043 eV) and $2p_{3/2}$ (1022 to 1020 eV) with rising temperature, indicating electron transfer from pyrrolic-N to Zn centers-consistent with Zn's electron-rich state (Figure S4). The XANES spectra (Figure 1E) indicate that ZnNC-800/900/1000 is situated between metallic Zn (0) and ZnTPP (+2), with higher pyrolysis temperatures causing a shift in electronic states toward Zn^0. EXAFS analysis (Figure 1E and 1F; Figures S5−S9) confirms the atomic dispersion of Zn, with no Zn−Zn pathways observed at 2.3 Å and Zn−N coordination detected at approximately 1.6 Å. This finding corroborates the results obtained from HADDF-STEM (Figure S2d). The increase in FT-EXAFS radius (from 1.48 Å to 1.63 Å) and the DFT-optimized ZnN_4 models (Figure 1G, H, Figures S5−S9, Tables S3−S7) reveal dynamic coordination environments, wherein pyridinic-N ligands are gradually replaced by pyrrolic-N (from Zn-Npd4 to Zn-Npo4). These configurations are denoted as Npd_npo_{4-n} (n = 0−4), with n representing the coordination number; pd and po refer to pyridinic and pyrrolic nitrogen atoms, respectively (Figure 1H). This trend is consistent with the XPS nitrogen speciation.[27,28] For example, ZnNC-600 is denoted as ZnNpd4, as the Zn center is coordinated by four pyridinic-N atoms, while ZnNC-900 is denoted as ZnNpd1po3, with coordination from one pyridinic-N atom and three pyrrolic-N atoms. Collectively, these findings demonstrate that the pyrolysis temperature plays a crucial role in tailoring the coordination and electronic structure of Zn, ultimately enhancing its catalytic performance.

Reaction Mechanism and Theoretical Calculation. To elucidate the reaction pathway, we investigated the transformations of three intermediates in Reaction (1)—1-(4-hydroxyphenyl)ethanone, 4-vinylphenol, and the amine addition product—under standard conditions. All three intermediates can be converted to phenol and DME (Figure 2A). In addition, when 4-(1-hydroxyethyl)phenol was used as the substrate, phenol was obtained in a yield of 47.6% (Reaction 5). The results indicate the existence of a reaction pathway where 1-(4-hydroxyphenyl)ethanone is converted to 4-(1-hydroxyethyl)phenol, subsequently to 4-vinylphenol, followed by the formation of an amine addition product, finally yielding the target products. The bond dissociation energies (BDEs) of the aryl-C(sp^2) σ-bonds in compounds **3a** and **4a** were calculated, showing that the BDE for **3a** is 8.73 eV, whereas for **4a** it is 4.93 eV (Table S8). This suggests that the addition of an amine lowers the bond dissociation energies of the C−C bond. Fourier transform infrared (FTIR) spectroscopy was used to investigate the adsorption behavior of 4-(1-aminoethyl)phenol on ZnNC-600 and ZnNC-900 catalysts (Figure 2B), revealing distinct interaction mechanisms. On ZnNC-900, a well-resolved doublet was observed at 1383 and 1370 cm^{-1}. Previous studies indicate that the symmetric bending ("umbrella") mode of a methyl group typically occurs near 1375 cm^{-1}, while isopropyl and *gem*-dimethyl groups give rise to a characteristic doublet in the regions 1385−1380 cm^{-1} and 1380−1370 cm^{-1},[29,30] with bands of similar intensity. Based on these references, the doublet on ZnNC-900 is attributed to a weak interaction between the amino group and the catalyst surface. This weak adsorption likely maintains the vibrational coupling of the $-CH_3$ umbrella mode, resulting in a clear splitting pattern similar to that observed in isopropyl-like systems. In contrast, a broad band spanning 1382−1370 cm^{-1}, rather than a resolved doublet, was observed for ZnNC-600. This suggests a stronger interaction between the adsorbate and the ZnNC-600 surface, which may involve partial protonation of the amino group. The resulting $-NH_3^+/NH_4^+$ species typically absorbs in the 1450−1400 cm^{-1} region,[31] and its low-wavenumber tail is likely to overlap with the $-CH_3$ bending region, masking the splitting and leading to the broadened spectral feature.

By combining XPS, XAFS, and IR analyses, we propose a mechanism illustrated in Figure 2C, which is further validated by Density Functional Theory (DFT) calculations. Computational details are provided in the Supporting Information. All energy values are referenced to the initial state comprising DMF, H_2O, 4-vinylphenol, and the catalyst, which is set to 0.00 eV in the potential energy surface. Initially, DMF undergoes hydrolysis in liquid phase, generating dimethylamine (DMA) and formic acid (HCOOH) (verified in Figure S10). DMA then reacts with 4-vinylphenol via a Michael addition-like process, forming an intermediate (**Int-1**) that undergoes tautomerization to form **Int-2**. Subsequently, **Int-2** interacts with Zn sites to form adsorbed intermediate **Int-3**, which undergoes aryl-C(sp^2) bond cleavage via the transition state **TS-1**. The energy barrier for this step is calculated to be 1.38 eV on ZnNpd1po3 (the structure corresponding to ZnNC-900), significantly lower than 2.09 eV on ZnNpd4 (the

https://doi.org/10.1021/jacs.5c10429
J. Am. Chem. Soc. 2025, 147, 37255−37264

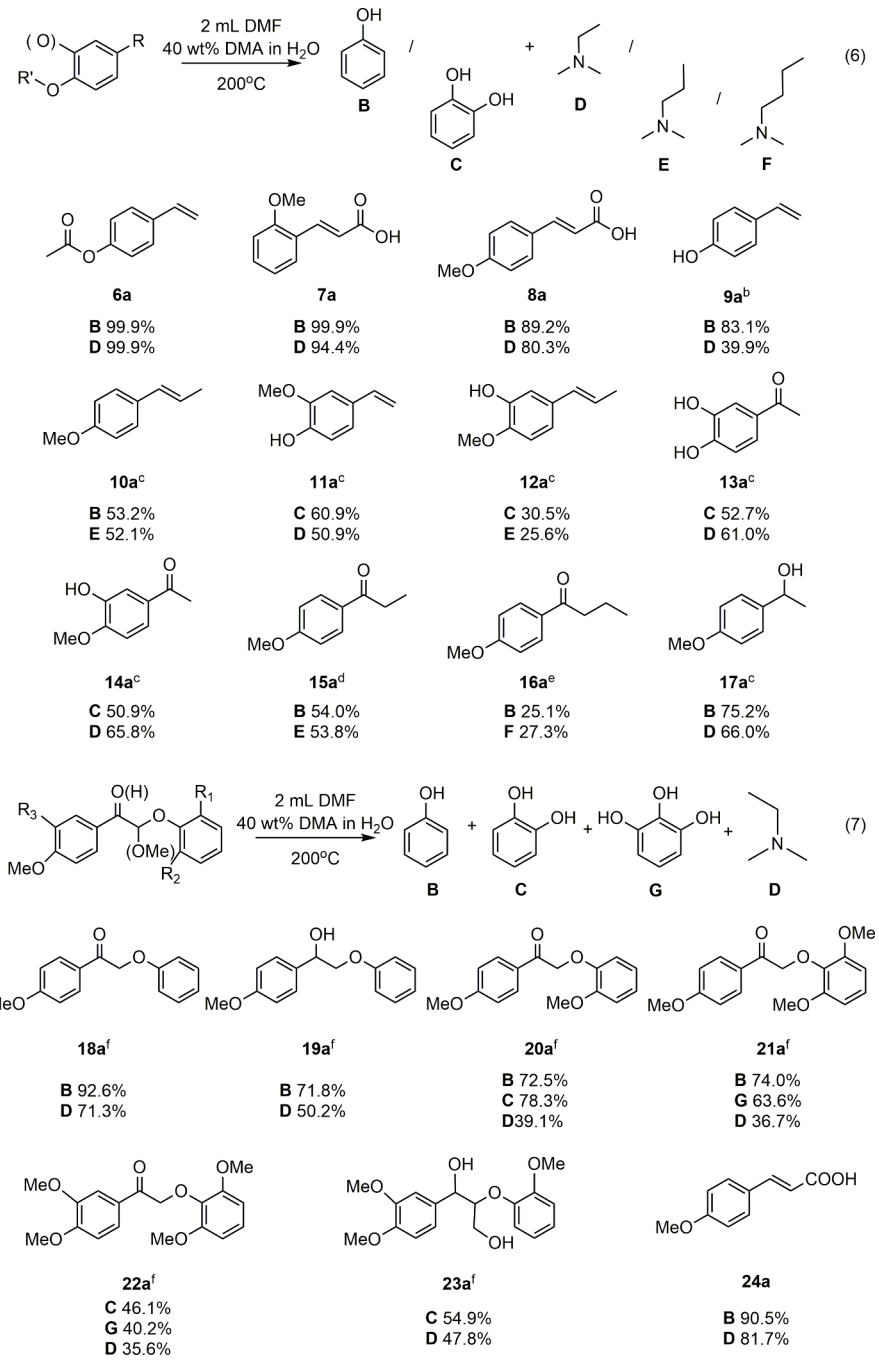

Figure 3. Substrate expansion.[a] Reaction conditions: substrate (0.4 mmol), ZnNC-900 (10 mg), DMF (2 mL), 40 wt % DMA in H_2O (2 mL), N_2 (1 MPa), 200 °C. [a]6 h. [b]2 h. [c]12 h. [d]14 h. [e]16 h. [f]20 h. 1 mol of substrate **17a** or **18a** reacts to yield 2 mol of phenol. The yield of product **C** was determined by HPLC, while the others are determined by GC with dodecane as an internal standard.

structure corresponding to ZnNC-600), correlating with the stronger adsorption energy of **Int-3** (−1.13 eV vs −0.44 eV). These findings are consistent with the observed IR spectrum and indicate that the Zn coordination environment critically influences the reactivity of the aryl-C bond. Electrostatic potential (ESP) mapping (Figure 2D) reveals that ZnNpd1po3 provides a more electron-rich environment around the Zn site compared to ZnNpd4. This electron enrichment enhances stabilization of the positively charged C═N^+ species in **TS-1** and promotes subsequent transformations. Subsequently, second transition states (**TS-2**/**TS-2′**) are identified for the reduction of Schiff base intermediate **Int-4**, leading to N,N-dimethylethylamine (DME) and CO_2 via an Eschweiler−Clarke-type mechanism. Formic acid plays a dual role: donating a proton to the phenoxide anion (to afford phenol) and serving as a hydride donor for C═N^+ reduction. The energy barriers for this step are 1.54 eV for ZnNpd1po3 and 1.62 eV for ZnNpd4, respectively. The enhanced stabilization of the Schiff base by the more electron-rich Zn site in ZnNpd1po3 explains the lower barrier and improved selectivity. These computational results are in good agreement with experimental data, showing that under identical conditions, ZnNC-900 (ZnNpd1po3) gives higher yields of phenol and DME than ZnNC-600 (ZnNpd4) (Figure S11).

https://doi.org/10.1021/jacs.5c10429
J. Am. Chem. Soc. 2025, 147, 37255−37264

Substrate Scope. The versatility of the ZnNC-900 catalytic system was assessed across a range of substrates including the aryl-C(sp^2) bond, encompassing variations in carbon chain lengths, substituents, and structural units derived from lignin (Figure 3). For phenethyl derivatives substituted with a single phenolic hydroxyl or methoxyl group, we observe relatively high yields of phenol and DME (compounds **6a**−**9a**). For example, for compounds **6a** and **7a**, the yield of phenol reached 99.9%, while the yield of DME exceeded 94%. However, the reactivity is slightly reduced for phenethyl derivatives with two phenolic hydroxyl (methoxyl) groups. For instance, in compound **11a**, the yield of catechol is 60.2% and the yield of DME decreases to 50.9%. Moreover, the length of the carbon chain associated with the aryl-C(sp^2) bond also affects the reactivity of the substrate. When the carbon chain is extended to three carbons, the yields of phenol and the corresponding amine drop to 53.2% and 52.1%, respectively (compound **10a**). In the case of compound **12a**, the yield of catechol is only 30.5%, while the yield of the corresponding amine is just 25.6%. For the conversion of phenyl ketone derivatives, a similar pattern was observed: the amount of substituted phenolic hydroxyl groups and the length of the carbon chain associated with the aryl-C(sp^2) bond both affect the reactivity of the substrate (compounds **13a**−**16a**). Although a yield of 90% for phenol and 82.7% for DME was achieved in phenyl ketone derivatives with a single phenolic hydroxyl group substitution (Table 1, entry 2), only a yield of 25.1% for phenol and 27.3% for DME was detected for compound **16a**. For the phenyl alcohol compound **17a**, the yields of phenol and DME also reached 75.2% and 66.0%, respectively.

Fortunately, this catalytic system also demonstrates efficient catalytic performance for typical model compounds of lignin (Compounds **18a**−**24a**, synthesis method shown in Figure S12). The lignin structure contains three common monomers: Guaiacyl (G-type monomer), Syringyl (S-type monomer), and p-hydroxyphenyl (H-type monomer). Regardless of whether it is the H-type monomer, S-type monomer, or G-type monomer, they can all be efficiently converted into the corresponding nonsubstituted phenolic compounds and DME. In comparison, the reactivity of the H-type monomer is higher. For example, in the case of compound **18a**, the yields of phenol and DME can reach 92.6% and 71.3%, respectively.

However, for monomers containing S-type and G-type structures, yields of phenol still exceed 70% (Compound **20a** and **21a**). For compound **20a**, the yield of catechol could reach 78.3%, and for compound **21a**, the yield of pyrogallol could reach 63.6%. The number of phenolic hydroxyl or methoxy groups on the aromatic ring associated with the aryl-C(sp^2) bond has a more significant impact on the reaction performance. For compounds **22a** and **23a**, the yields of both phenols drop below 60%. Compound **24a**, a representative of the p-coumaric acid unit in lignin, was selectively converted to phenol and dimethylamine (DME) with respective yields of 90.5% and 81.7%.

Furthermore, we explored the reactivity of various secondary amines. Both N-ethylmethylamine and diethylamine facilitated the formation of the corresponding phenolic and tertiary amine products (Figure 4). When N-ethylmethylamine served as the nitrogen source, yields of 36.2% phenol and 36.5% N N-diethylmethylamine were achieved (Reaction 8). Conversely, using diethylamine as the nitrogen source resulted in the conversion of 1-(4-methoxy-phenyl)-2-phenoxy-ethanone to

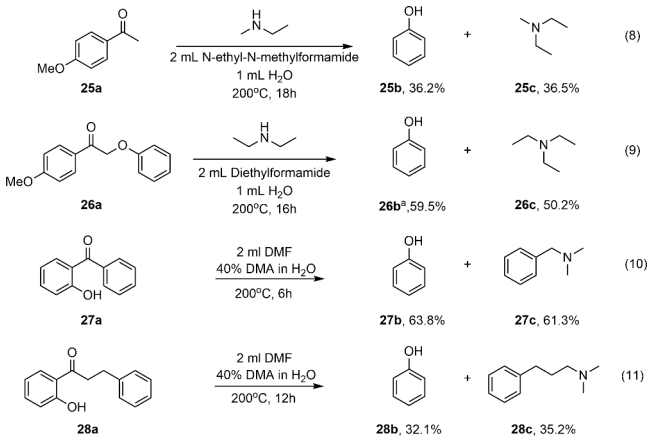

Figure 4. Nitrogen source influence. Reaction conditions: substrate (0.4 mmol), ZnNC-900 (10 mg), amide (2 mL), secondary amine (1 mL) H_2O (1 mL), N_2 (1 MPa), 200 °C. [a]1 mol of substrate reacts to yield 2 mol of phenol.

59.5% phenol and 50.2% triethylamine, which is an important bulk chemical (Reaction 9). For the transformation of **27a** and **28a**, corresponding arylalkyl amines were obtained (Reaction 10 and 11). When hydroxyl was substituted by halogens or nitro groups, aryl-C(sp^2) bond cleavage products were not detected (Figure S13).

Building on the reactivity observed with typical lignin-derived monomers, various native lignins were extracted from various biomass sources—including bamboo, corn straw, peanut shells, poplar wood, and xylose residue—and subjected to the reaction system (Figures S14 to S15). As summarized in Table 3, all tested lignins were effectively transformed into phenols and DME under the optimized reaction conditions. Notably, bamboo lignin achieved a total phenolic yield of 12.9 wt % (Table 3, entry 1; Figure S14), consisting of 7.9 wt % phenol, 1.6 wt % catechol, and 3.4 wt % pyrogallol, along with a DME yield of 15.0 wt %. A comparative analysis of the heteronuclear single quantum correlation (HSQC) spectra before and after the reaction showed a nearly complete disappearance of the β-O-4 region, confirming the consumption of these side chains (see Figure S14). To further evaluate the method's industrial viability, a scaled-up experiment was conducted with bamboo lignin over 24 h. From 5.0 g of lignin, 1.04 g of alkyl-free phenolic compounds were obtained, composed of 38% phenol (Figure S16, Figure S19), 22% catechol, and 40% pyrogallol, alongside 13.4% mass yield of DME (0.67 g) (Table 3, entry 6; Figure S17, Figure S20). Strikingly, these results surpass the initial pilot-scale performance. Collectively, this work demonstrates a robust and scalable catalytic strategy for lignin valorization, bridging fundamental innovation with industrial practicality.

CONCLUSIONS

In summary, we have developed a catalytic strategy that addresses the long-standing challenge of selectively cleaving inert aryl-C(sp^2) σ-bonds under mild conditions, enabling the concurrent valorization of aromatic nuclei and alkyl side chains of lignin. The ZnNC-900 catalyst, with its electron-rich Zn centers embedded in a nitrogen-doped carbon matrix, achieves high efficiency by stabilizing critical intermediates and lowering activation energy. This approach not only can convert model lignin compounds into high-value phenols and alkyl amines

https://doi.org/10.1021/jacs.5c10429
J. Am. Chem. Soc. 2025, 147, 37255−37264

Table 3. Conversion of Different Types of Lignin into Phenols and DME[a]

Entry	Types	Yield (wt %)		
		Phenols[c]		DME
1	Bamboo lignin	12.9	7.9 (Phenol) 1.6 (Catechol) 3.4 (Pyrogallol)	15.0
2	Straw lignin	6.5	3.5 (Phenol) 2.8 (Catechol) 0.2 (Pyrogallol)	7.7
3	Peanut shell lignin	1.7	0.6 (Phenol) 1.0 (Catechol) 0.1 (Pyrogallol)	12.7
4	Poplar lignin	5.3	1.5 (Phenol) 0.7 (Catechol) 3.1 (Pyrogallol)	6.4
5	Xylose residue	5.5	3.1 (Phenol) 1.8 (Catechol) 0.6 (Pyrogallol)	4.3
6[b]	Bamboo lignin	20.8	8.0 (Phenol) 4.4 (Catechol) 8.4 (Pyrogallol)	13.4

[a]Reaction condition: lignin (100 mg), ZnNC-900 (15 mg), DMF (3 mL), 40 wt % DMA in water (3 mL), N_2 (1 MPa), 200 °C, 20 h. Mass yield (%) = $\frac{m_x}{m_o} \times 100\%$. Here, m_x represents the mass of corresponding product, and m_0 represents the original mass of lignin. [b]Lignin (5.0 g), ZnNC-900 (0.7 g), DMF (100 mL), 40 wt % DMA in water (100 mL), N_2 (1 MPa), 200 °C, 24 h. [c]The yields of phenolic products are presented as total phenol yield (left column) and individual phenol yields (right column).

with >90% selectivity but also can convert native lignin from diverse biomass sources into renewable aromatics and amines, circumventing carbon loss as CO_2 or alkanes. A scaled-up experiment using native lignin validated the scalability of the process, showing its potential for industrial application. By integration of mechanistic insights from advanced spectroscopy and theoretical calculation, the role of Zn−N coordination in mediating bond cleavage and functionalization is elucidated. This work provides a strategy to cleave inert aryl-C(sp^2) σ-bonds and convert lignin with high atomic efficiency.

■ ASSOCIATED CONTENT

Supporting Information

The Supporting Information is available free of charge at https://pubs.acs.org/doi/10.1021/jacs.5c10429.

Additional references within the Supporting Information; Additional data and methodology details include experimental procedures, characterization of catalysts, cycling stability data, HSQC NMR spectra for products, GC-MS and LC-MS spectra for representative products (phenol, N,N-dimethylethylamine, N-containing intermediate, catechol, pyrogallol), XAFS fitting results and supplementary figures and tables (PDF)

■ AUTHOR INFORMATION

Corresponding Author

Huizhen Liu − *Beijing National Laboratory for Molecular Sciences, CAS Laboratory of Colloid and Interface and Thermodynamics, CAS Research/Education Center for Excellence in Molecular Sciences, Center for Carbon Neutral Chemistry, Institute of Chemistry, Chinese Academy of Sciences (CAS), Beijing 100190, China; School of Chemical Sciences, University of Chinese Academy of Sciences, Beijing 100049, China;* orcid.org/0000-0002-6801-7816; Email: liuhz@iccas.ac.cn

Authors

Lulin Wang − *Beijing National Laboratory for Molecular Sciences, CAS Laboratory of Colloid and Interface and Thermodynamics, CAS Research/Education Center for Excellence in Molecular Sciences, Center for Carbon Neutral Chemistry, Institute of Chemistry, Chinese Academy of Sciences (CAS), Beijing 100190, China; School of Chemical Sciences, University of Chinese Academy of Sciences, Beijing 100049, China*

Yike Huang − *Electronic design automation center, Institute of microelectronics of Chinese Academy of Sciences, Beijing 100029, China*

Yu Xin − *Beijing National Laboratory for Molecular Sciences, CAS Laboratory of Colloid and Interface and Thermodynamics, CAS Research/Education Center for Excellence in Molecular Sciences, Center for Carbon Neutral Chemistry, Institute of Chemistry, Chinese Academy of Sciences (CAS), Beijing 100190, China; School of Chemical Sciences, University of Chinese Academy of Sciences, Beijing 100049, China*

Tianjiao Wang − *Beijing National Laboratory for Molecular Sciences, CAS Laboratory of Colloid and Interface and Thermodynamics, CAS Research/Education Center for Excellence in Molecular Sciences, Center for Carbon Neutral Chemistry, Institute of Chemistry, Chinese Academy of Sciences (CAS), Beijing 100190, China; School of Chemical Sciences, University of Chinese Academy of Sciences, Beijing 100049, China*

Sen Luan − *Beijing National Laboratory for Molecular Sciences, CAS Laboratory of Colloid and Interface and Thermodynamics, CAS Research/Education Center for Excellence in Molecular Sciences, Center for Carbon Neutral Chemistry, Institute of Chemistry, Chinese Academy of Sciences (CAS), Beijing 100190, China; School of Chemical Sciences, University of Chinese Academy of Sciences, Beijing 100049, China*

Minghua Dong − *Beijing National Laboratory for Molecular Sciences, CAS Laboratory of Colloid and Interface and Thermodynamics, CAS Research/Education Center for Excellence in Molecular Sciences, Center for Carbon Neutral Chemistry, Institute of Chemistry, Chinese Academy of Sciences (CAS), Beijing 100190, China; School of Chemical Sciences, University of Chinese Academy of Sciences, Beijing 100049, China*

Bin Zhang − *Beijing National Laboratory for Molecular Sciences, CAS Laboratory of Colloid and Interface and Thermodynamics, CAS Research/Education Center for Excellence in Molecular Sciences, Center for Carbon Neutral Chemistry, Institute of Chemistry, Chinese Academy of Sciences (CAS), Beijing 100190, China;* orcid.org/0000-0003-3172-8056

Xiaojun Shen − *Department School of Chemical Sciences, State Key Laboratory of Efficient Production of Forest Resources, Beijing Forestry University, Beijing 100083, China;* orcid.org/0000-0001-5626-3991

Qinglei Meng − *Beijing National Laboratory for Molecular Sciences, CAS Laboratory of Colloid and Interface and*

Thermodynamics, CAS Research/Education Center for Excellence in Molecular Sciences, Center for Carbon Neutral Chemistry, Institute of Chemistry, Chinese Academy of Sciences (CAS), Beijing 100190, China

Buxing Han − *Beijing National Laboratory for Molecular Sciences, CAS Laboratory of Colloid and Interface and Thermodynamics, CAS Research/Education Center for Excellence in Molecular Sciences, Center for Carbon Neutral Chemistry, Institute of Chemistry, Chinese Academy of Sciences (CAS), Beijing 100190, China; School of Chemical Sciences, University of Chinese Academy of Sciences, Beijing 100049, China;* orcid.org/0000-0003-0440-809X

Complete contact information is available at: https://pubs.acs.org/10.1021/jacs.5c10429

Author Contributions

[#]L.W. and Y.H. contributed equally.

Notes

The authors declare no competing financial interest.

■ ACKNOWLEDGMENTS

This work received financial support from National Key Research and Development Program of China (2022YFA1504901), National Natural Science Foundation of China (22179132, 22293012, 22072157 and 22121002) and Youth Fund of National Natural Science Foundation (223002209).

■ REFERENCES

(1) Liang, Y.-F.; Bilal, M.; Tang, L.-Y.; Wang, T.-Z.; Guan, Y.-Q.; Cheng, Z.; Zhu, M.; Wei, J.; Jiao, N. Carbon-Carbon Bond Cleavage for Late-Stage Functionalization. *Chem. Rev.* **2023**, *123* (22), 12313−12370.

(2) Wang, J.; Wei, D.; Duan, Z.; Mathey, F. Cleavage of the Inert C(sp^2)-Ar σ-Bond of Alkenes by a Spatial Constrained Interaction with Phosphinidene. *J. Am. Chem. Soc.* **2020**, *142* (50), 20973−20978.

(3) Cheng, Z.; Huang, K.; Wang, C.; Chen, L.; Li, X.; Hu, Z.; Shan, X.; Cao, P.-F.; Sun, H.; Chen, W.; Li, C.; Zhang, Z.; Tan, H.; Jiang, X.; Zhang, G.; Zhang, Z.; Lin, M.; Wang, L.; Zheng, A.; Xia, C. Catalytic Remodeling of Complex Alkenes to Oxonitriles through C = C Double Bond Deconstruction. *Science* **2025**, *387* (6738), 1083−1090.

(4) He, Y.; Zeng, X.; Lu, Z.; Mo, S.; An, Q.; Liu, Q.; Yang, Y.; Lan, W.; Wang, S.; Zou, Y. Aqueous Electrocatalytic Hydrogenation Depolymerization of Lignin β-O-4 Linkage via Selective c_{aryl}-O(C) Bond Cleavage: The Regulation of Adsorption. *J. Am. Chem. Soc.* **2024**, *146* (46), 32022−32031.

(5) Kalsoom, I.; Bilal, M.; Kanwal, A.; Rasool, N.; Nazeer, U.; Ciurea, C.; Elena Neculau, A.; Constantina Martinescu, C. Selective C-c Bond Cleavage of Cycloketoximes via Iminyl Radicals and Distal Carbon Radicals through Photocatalysis. *J. Saudi Chem. Soc.* **2024**, *28* (3), 101848.

(6) Zhang, R.; Zhang, J.; Liu, H.; Jiang, Z.; Liu, X.; Wang, W.; Peng, L.; Hu, C. Toward Value-Added Chemicals from Carbohydrates via C-C Bond Cleavage and Coupling Transformations. *ACS catal.* **2024**, *14* (7), 5167−5197.

(7) Baek, D.; Al Abdulghani, A. J.; Walsh, D. J.; Hofsommer, D. T.; Gerken, J. B.; Shi, C.; Chen, E. Y.-X.; Hermans, I.; Stahl, S. S. Can the Hock Process Be Used to Produce Phenol from Polystyrene? *J. Am. Chem. Soc.* **2025**, *147*, 8687−8694.

(8) Ao, Y.; Wang, N.; Tang, S.-Y.; Wang, Z.-J.; Zou, L.-H.; Huang, H.-M. Enantioselective Remote Alkylation Enabled by Metallaphotoredox Catalysis via Selective C-c Bond Cleavage. *ACS Catal.* **2025**, *15* (3), 2212−2221.

(9) Huang, Z.; Guan, R.; Shanmugam, M.; Bennett, E. L.; Robertson, C. M.; Brookfield, A.; McInnes, E. J. L.; Xiao, J. Oxidative Cleavage of Alkenes by O_2 with a Non-Heme Manganese Catalyst. *J. Am. Chem. Soc.* **2021**, *143* (26), 10005−10013.

(10) Li, L.; Li, Z.-L.; Gu, Q.-S.; Wang, N.; Liu, X.-Y. A Remote C-C Bond Cleavage-Enabled Skeletal Reorganization: Access to Medium-/Large-Sized Cyclic Alkenes. *Sci. Adv.* **2017**, *3* (11), No. e1701487.

(11) Wang, Z.-Y.; Wang, S.; Dai, N.-N.; Xiao, Y.; Zhou, Y.; Tian, W.-C.; Sun, D.; Li, Q.; Wang, Y.; Wei, W.-T. Carbon-Carbon Triple Bond Cleavage and Reconstitution to Achieve Aryl Amidation Using Nitrous Acid Esters. *Nat. Commun.* **2025**, *16* (1), 993.

(12) Liu, Z.-H.; Liu, H.; Xu, T.; Zhao, Z.-M.; Ragauskas, A. J.; Li, B.-Z.; Yuan, J. S.; Yuan, Y.-J. Lignin Valorization Reshapes Sustainable Biomass Refining. *Renew. and Sust. Energy Rev.* **2025**, *211*, 115296.

(13) Yu, Z.; Kong, W.; Liang, W.; Guo, Y.; Cui, J.; Hu, Y.; Sun, Z.; Elangovan, S.; Xu, F. Heterogeneously Catalyzed Reductive Depolymerization of Lignin to Value-Added Chemicals. *ChemSusChem* **2025**, *18*, No. e202401399.

(14) Ragauskas, A. J.; Beckham, G. T.; Biddy, M. J.; Chandra, R.; Chen, F.; Davis, M. F.; Davison, B. H.; Dixon, R. A.; Gilna, P.; Keller, M.; Langan, P.; Naskar, A. K.; Saddler, J. N.; Tschaplinski, T. J.; Tuskan, G. A.; Wyman, C. E. Lignin Valorization: Improving Lignin Processing in the Biorefinery. *Science* **2014**, *344* (6185), 1246843−1246843.

(15) Bomon, J.; Van Den Broeck, E.; Bal, M.; Liao, Y.; Sergeyev, S.; Van Speybroeck, V.; Sels, B. F.; Maes, B. U. W. Brønsted Acid Catalyzed Tandem Defunctionalization of Biorenewable Ferulic Acid and Derivates into Bio-Catechol. *Angew. Chem., Int. Ed.* **2020**, *59* (8), 3063−3068.

(16) Tian, X.-R.; Jiang, Z.-Y.; Hou, S.-L.; Hu, H.-S.; Li, J.; Zhao, B. A Strong-Acid-Resistant [Th_6] Cluster-Based Framework for Effectively and Size-Selectively Catalyzing Reductive Amination of Aldehydes with *N*, *N*-Dimethylformamide. *Angew. Chem., Int. Ed.* **2023**, *62* (23), No. e202301764.

(17) Sethupathy, S.; Murillo Morales, G.; Gao, L.; Wang, H.; Yang, B.; Jiang, J.; Sun, J.; Zhu, D. Lignin Valorization: Status, Challenges and Opportunities. *Bioresour. Technol.* **2022**, *347*, 126696.

(18) Baron, C. *Phenol market volume worldwide 2024 | Statista.* Statista. https://www.statista.com/statistics/979265/global-phenol-market-volume/ (Accessed 2025-08-25).

(19) Li, Q.; Long, Y.; Tao, Q.; Jin, Z.; Yan, X.; Zhou, X. Palladium-Catalyzed C(O)-C Bond Cleavage of Unstrained Ketones Assisted with Aryl Handles: An Approach to Diaryl Ketones. *Org. Lett.* **2025**, *27*, 2758−2763.

(20) Liao, Y.; Koelewijn, S.-F.; Van den Bossche, G.; Van Aelst, J.; Van den Bosch, S.; Renders, T.; Navare, K.; Nicolaï, T.; Van Aelst, K.; Maesen, M.; Matsushima, H.; Thevelein, J. M.; Van Acker, K.; Lagrain, B.; Verboekend, D.; Sels, B. F. A Sustainable Wood Biorefinery for Low-Carbon Footprint Chemicals Production. *Science* **2020**, *367* (6484), 1385−1390.

(21) Yan, J.; Meng, Q.; Shen, X.; Chen, B.; Sun, Y.; Xiang, J.; Liu, H.; Han, B. Selective Valorization of Lignin to Phenol by Direct Transformation of C_{sp2} -C_{sp3} and C-O Bonds. *Sci. Adv.* **2020**, *6* (45), No. eabd1951.

(22) Wang, M.; Liu, M.; Li, H.; Zhao, Z.; Zhang, X.; Wang, F. Dealkylation of Lignin to Phenol via Oxidation-Hydrogenation Strategy. *ACS Catal.* **2018**, *8* (8), 6837−6843.

(23) Shen, X.; Meng, Q.; Mei, Q.; Liu, H.; Yan, J.; Song, J.; Tan, D.; Chen, B.; Zhang, Z.; Yang, G.; Han, B. Selective Catalytic Transformation of Lignin with Guaiacol as the Only Liquid Product. *Chem. Sci.* **2020**, *11* (5), 1347−1352.

(24) Wang, T.; Xin, Y.; Chen, B.; Zhang, B.; Luan, S.; Dong, M.; Wu, Y.; Cheng, X.; Liu, Y.; Liu, H.; Han, B. Selective Hydrodeoxygenation of α, β-Unsaturated Carbonyl Compounds to Alkenes. *Nat. Commun.* **2024**, *15* (1), 2166.

(25) Xie, C.; Lin, L.; Huang, L.; Wang, Z.; Jiang, Z.; Zhang, Z.; Han, B. Zn-Nx Sites on N-Doped Carbon for Aerobic Oxidative Cleavage and Esterification of C(CO)-C Bonds. *Nat. Commun.* **2021**, *12* (1), 4823.

(26) Li, J.; Li, C.; Feng, S.; Zhao, Z.; Zhu, H.; Ding, Y. Atomically Dispersed Zn-N $_x$ Sites in N-Doped Carbon for Reductive N-Formylation of Nitroarenes with Formic Acid. *ChemCatChem.* **2020**, *12* (6), 1546−1550.
(27) Peng, W.; Liu, J.; Liu, X.; Wang, L.; Yin, L.; Tan, H.; Hou, F.; Liang, J. Facilitating Two-Electron Oxygen Reduction with Pyrrolic Nitrogen Sites for Electrochemical Hydrogen Peroxide Production. *Nat. Commun.* **2023**, *14* (1), 4430.
(28) Inagaki, M.; Toyoda, M.; Soneda, Y.; Morishita, T. Nitrogen-Doped Carbon Materials. *Carbon* **2018**, *132*, 104−140.
(29) Asemani, M.; Rabbani, A. R. Detailed FTIR Spectroscopy Characterization of Crude Oil Extracted Asphaltenes: Curve Resolve of Overlapping Bands. *J. Petrol. Sci. Eng.* **2020**, *185*, 106618.
(30) Colthup, N. B.; Fateley, W. G.; Grasselli, J. G.; Lin-Vien, D. Chapter 2: Alkanes. *The Handbook of Infrared and Raman Characteristic Frequencies of Organic Molecules*; Academic Press: Boston, MA, 1991.
(31) Pironon, J.; Pelletier, M.; De Donato, P.; Mosser-Ruck, R. Characterization of Smectite and Illite by FTIR Spectroscopy of Interlayer NH4+ Cations. *Clay Miner.* **2003**, *38* (2), 201−211.

https://doi.org/10.1021/jacs.5c10429
J. Am. Chem. Soc. 2025, 147, 37255−37264